doi:10.1016/j.jmb.2004.11.052 J. Mol. Biol. (2005) 346, 267–277

JMB

Available online at www.sciencedirect.com

SCIENCE DIRECT®

ELSEVIER

Structure of the Mature P3-virus Particle Complex of Cauliflower Mosaic Virus Revealed by Cryo-electron Microscopy

Célia Plisson[1]†, Marilyne Uzest[2]†, Martin Drucker[2], Rémy Froissart[2] Christian Dumas[3], James Conway[4], Daniel Thomas[1], Stéphane Blanc[2] and Patrick Bron[1]*

[1]*Université Rennes I, UMR 6026 CNRS, Campus de Beaulieu, 35042 Rennes, France*

[2]*Station de Recherches de Pathologie Comparée, UMR 1231, INRA-CNRS-Université Montpellier II, 30380 Saint-Christol-les-Alès, France*

[3]*Centre de Biochimie Structurale, UMR CNRS 5048 UMR 554 INSERM, Université Montpellier I, France*

[4]*Laboratoire de Microscopie Electronique, Institut de Biologie Structurale J.-P. Ebel Grenoble 38027, France*

**Corresponding author*

The cauliflower mosaic virus (CaMV) has an icosahedral capsid composed of the viral protein P4. The viral product P3 is a multifunctional protein closely associated with the virus particle within host cells. The best-characterized function of P3 is its implication in CaMV plant-to-plant transmission by aphid vectors, involving a P3–virion complex. In this transmission process, the viral protein P2 attaches to virion-bound P3, and creates a molecular bridge between the virus and a putative receptor in the aphid's stylets. Recently, the virion-bound P3 has been suggested to participate in cell-to-cell or long-distance movement of CaMV within the host plant. Thus, as new data accumulate, the importance of the P3–virion complex during the virus life-cycle is becoming more and more evident. To provide a first insight into the knowledge of the transmission process of the virus, we determined the 3D structures of native and P3-decorated virions by cryo-electron microscopy and computer image processing. By difference mapping and biochemical analysis, we show that P3 forms a network around the capsomers and we propose a structural model for the binding of P3 to CaMV capsid in which its C terminus is anchored deeply in the inner shell of the virion, while the N-terminal extremity is facing out of the CaMV capsid, forming dimers by coiled-coil interactions. Our results combined with existing data reinforce the hypothesis that this coiled-coil N-terminal region of P3 could coordinate several functions during the virus life-cycle, such as cell-to-cell movement and aphid-transmission.

Keywords: CaMV/P3; protein structure; cryo-electron microscopy; icosahedral reconstruction; aphid-transmission

Introduction

Cauliflower mosaic virus (CaMV) is the type member of the family Caulimoviridae (genus *Caulimovirus*) which, together with hepadnaviruses, constitute the para-phylletic group of pararetroviruses having a DNA-based genome replicated *via* reverse transcription of a pre-genomic RNA.[1,2] The approximately 8 kbp circular double-stranded DNA genome of CaMV encodes eight major open reading frames (ORFs). To the products of six ORFs at least one biological function has been assigned.[3] ORF I encodes P1, a protein involved in cell-to-cell movement and systemic spread of the virus within the host. ORFs II and III are described in further detail below as their products (P2 and P3) form a complex with virus particles to promote plant-to-plant vector-transmission, currently the only biological function demonstrated experimentally for the P3–virion complex. ORF IV codes for the precursor of the coat protein (57 kDa), which is post-translationally processed into variable amounts of three major forms of P4 with molecular mass ranging between 35 kDa and 44 kDa. The reverse transcriptase replicating the genome is encoded by ORF V. ORF VI directs the expression of a multifunctional protein, P6, that constitutes the

† C.P. & M.U. contributed equally to this work.

Abbreviations used: CaMV, cauliflower mosaic virus; ORF, open reading frame; edIB, electron-dense inclusion bodies; elIB, electron-lucent inclusion bodies.

E-mail address of the corresponding author: patrick.bron@univ-rennes1.fr

matrix of the electron-dense inclusion bodies and transactivates the translation of the other ORFs from the viral 35 S RNA or its spliced forms.[4] The biological significance of the two additional ORFs, VII and VIII, is unclear, as no corresponding protein products have been detected in infected plants.

CaMV forms icosahedral virus particles, 50 nm in diameter, the viral DNA being tightly associated with the inner side of the protein shell.[5] More precisely, the icosahedron is organized with a $T=7$ symmetry forming three concentric layers around a large, solvent-filled cavity.[6] The outermost layer of the virion shell contains 420 P4 molecules that form 72 capsomeric morphological units, with 12 pentamers and 60 hexamers. The circular DNA is thought to be enclosed within the intermediate and the innermost layers of the viral capsid.[7]

For a long time, the role of P3 in the viral cycle was unclear. Apart from a short, central region composed of 20 amino acid residues, all P3 sequences are required for CaMV infectivity.[8] A DNA-binding activity has been identified,[9,10] and has been mapped to the C-terminal extremity of P3,[11] but, despite the fact that this DNA-binding domain is required for CaMV infectivity, its role during CaMV infection is not known. So the full-length P3 (15 kDa), or a putative processed product (11 kDa), was believed to be a minor structural protein component of the virion shell.[9,10,12] It is supported by immunolocalization of P3 in infected plants, which showed that the virus particles are always found together with P3.[13] A strong affinity between virions and P3 has been demonstrated,[14,15] and has been quantified *in vitro*.[13,16] The domain of P3 involved in virion binding is located in a large C-terminal region, and P3 has been shown to bind both to mature virions and to unassembled coat protein.[14]

However, recent results have suggested further non-structural roles for P3. On the one hand, P3 was demonstrated to be totally separated from virus particles upon purification,[15] to be dispensable for forming correctly shaped virions,[17] and to accumulate in infected cells with virions in electron-dense inclusion bodies (edIB), and in electron-lucent inclusion bodies (elIB).[13] On the other hand, P3 seems to play a role in the vector transmission, which implies formation of the P3–virion complex. Aphids transmit CaMV in a non-circulative manner, meaning that the virus particles are acquired in infected plants and specifically retained in the food canal of the aphid's stylets. From there, they are subsequently released and inoculated in a new host plant. The molecular mechanisms behind this seemingly simple process are highly sophisticated in CaMV and have been characterized extensively.[18] The relevance of P3–virion complexes was highlighted in a series of works[13–15] demonstrating that P2 (ORF II product) attaches first to the stylets, and can subsequently interact with, and retain, P3 previously bound to virions and acquired by the aphid during additional probing. Thus, the complete transmissible P2–P3–virion complex forms in the aphid stylets and not in infected plant cells, whereas P3–virion complexes accumulate in electron-dense inclusion bodies, and P2 is stored apart in elIB.[13] P2-free P3–virion complexes were detected in vascular tissues,[16] suggesting that they may represent the form of CaMV colonizing its host plant. In agreement, it has been demonstrated that ORF III-deleted CaMV replicates in protoplasts,[17] suggesting that P3 is required for cell-to-cell and/or long distance movement, rather than for replication.

While the numerous properties of P3 and its roles in the CaMV life-cycle remain poorly understood, the importance of P3–virion complexes is becoming more evident as new data accumulate. However, the structure of this complex, the form of P3 involved, the stoichiometry P3/P4 and the sites of P3 attachment onto virus particles remain totally unknown.

Here, we have determined the three-dimensional structures of native CaMV and P3-decorated CaMV capsids by cryo-electron microscopy and image processing. The difference map between native and P3-decorated virions reveals extra densities localised in the outermost layer that also reach into the intermediate layer. We show that the P3 N-terminal region is accessible to solvent, whereas the C-terminal extremity is anchored into the viral capsid. On the basis of our results, combined with previously reported biochemical and biological data, we propose a structural model of the P3–virion complex. This model is discussed with regard to the structure-function relationship of P3 and its plausible role in selectively controlling various pathways in the virus life-cycle, such as movement within and transmission between hosts.

Results

Reconstitution of the P3–virion complex

CaMV particles and P3 were incubated for between 24 hours and 48 hours at 4 °C with gentle stirring. As shown in Figure 1, large amounts of P3 subsequently sedimented together with virions, thus likely forming P3–virion complexes. Interestingly, some P3 was still present in solution in the supernatant, suggesting that saturation of CaMV particles with P3 had been reached. This excess of soluble P3 appeared with P3/P4 molecular ratios between 1 : 1 and 2 : 1 (data not shown); therefore, imaging of P3–CaMV particle complexes in cryo-electron microscopy was performed with a molecular ratio of 1.5 : 1 as described in Materials and Methods. Due to agregation of P3–CaMV particle complexes during centrifugation, excess of free P3 was not removed. Figure 2 shows typical micrographs of unstained, frozen-hydrated native and P3-decorated CaMV virions. In both cases, virus particles have a circular shape of about 530 Å in diameter and appear morphologically similar. In the micrograph of P3-decorated CaMV virions, a background of small particles is observed.

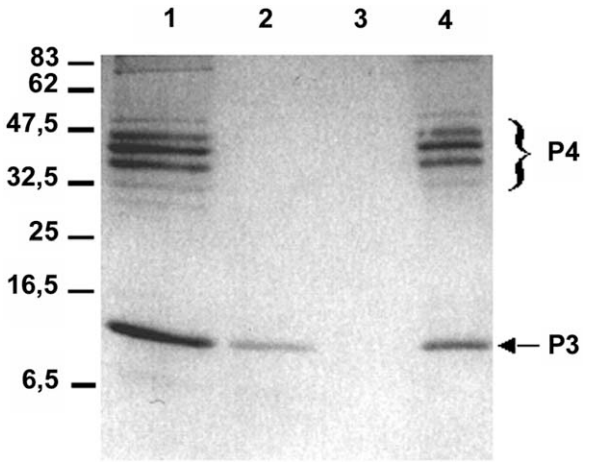

Figure 1. Visualization of P3:CaMV complexes by SDS-PAGE. Purified P3 and virions were mixed at a molar ratio of 1.5 : 1, to reconstitute complexes *in vitro* as indicated in Materials and Methods. After 24–48 hours of gentle stirring at 4 °C, the complexes were sedimented at 100,000 *g* for three hours and resuspended in the initial volume of CaMV buffer. Samples (10 µl) of each fraction were submitted to SDS/15% PAGE and the proteins were stained with Coomassie brilliant blue. The gel was loaded as follows: lane 1, mixture of P3 and virions at about 1 mg/ml (total protein concentration) before centrifugation; lanes 2 and 3, supernatants of ultracentrifugation step and rinse of the pellet, respectively; lane 4, resuspended pellet. The molecular mass marker scale is indicated at the left.

Nevertheless, micrographs were exploitable for image processing.

Three-dimensional density maps

Three-dimensional maps of native and P3-decorated CaMV particles were computed using a model-based orientation determination method.[19] A total of 653 images of CaMV and 1484 images of P3–virion complexes were included in the two final 3D reconstructions, both computed to 26 Å resolution. Because the reconstructions were computed from independent micrographs, corrections for magnification differences and for contrast transfer function (CTF) were necessary before calculating a difference map between reconstructions. These corrections ensure that the differences between the reconstructions are structural, and are not the result of imaging conditions. Plots of the normalised average radial density for native and P3-decorated CaMV reconstructions are presented in Figure 3. Although the 125 Å density peak corresponds to small protrusions of density of the innermost layer that radiate toward the solvent-filled virion center, it is quite sensitive to residual noise. Then, we decided to use the 155 Å density peak as reference for normalising intensities of the P3-decorated CaMV map. Normalisation using a least-squares method gives notably the same result. The multilayer nature of the viral particle is revealed clearly in both reconstructions. The binding of P3 onto CaMV capsid induces a relative increase of density with a lateral shift of the peak position for the outermost and intermediate layers to higher radius values. This reflects a swelling of the capsid upon

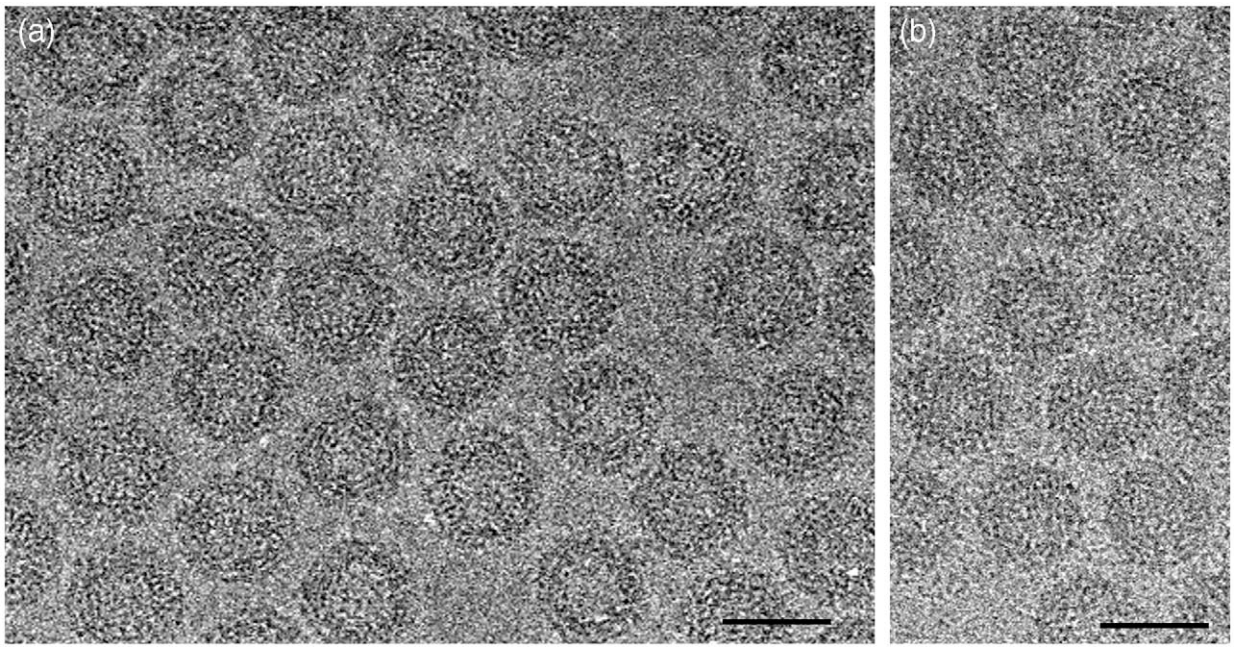

Figure 2. Micrographs of unstained specimens of native and P3-decorated CaMV. Micrographs were recorded with a JEOL 2010F microscope operating at 200 kV and 39, 600× magnification. (a) CaMV with defocus $\Delta = -2.8$ µm. (b) P3–CaMV complexes with defocus $\Delta = -2.5$ µm. The scale bar represents 50 nm.

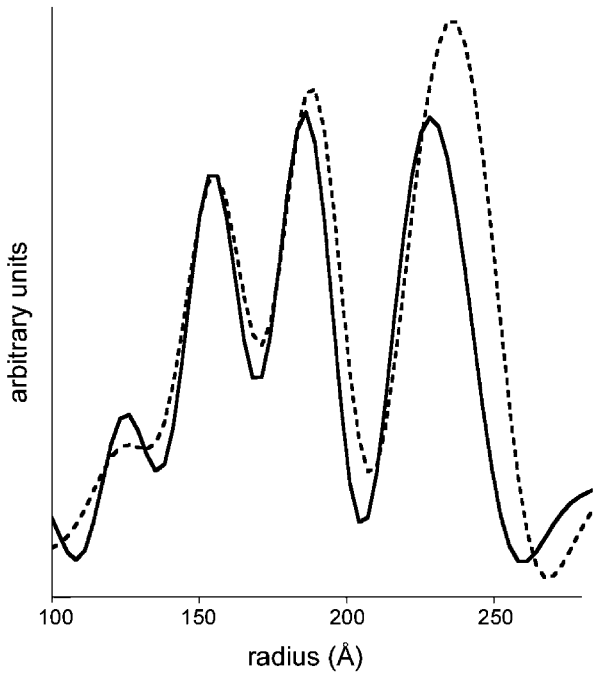

Figure 3. Plots of the average radial density. Radial density plots of the CaMV reconstruction (continuous line) and P3–CaMV complex reconstruction (broken line). In both reconstructions, three layers are clearly resolved. The small peak at a radius of 125 Å corresponds to small protrusions of density of the innermost layer that radiate toward the solvent-filled virion center. The plots were normalized by using the density peak located at 155 Å as reference.

P3 binding. The structural parameters are summarised in Table 1. The swelling factors are not identical between the outermost and intermediate layers.

Surface representations, transversal sections and radial projections are presented in Figure 4. In both reconstructions, the viral particle is an icosahedral virion with $T=7$ symmetry and is composed of three concentric protein layers. The outermost layer consists of 72 capsomers arranged in 60 hexamers and 12 pentamers.

In the reconstruction of native CaMV, the structural domains are notably well defined, as attested by the clear delineation of the capsomers of the outermost layer. Capsomers are surrounded by pores, which penetrate the outermost layer. Although represented at the same resolution, the 3D reconstruction of the P3–virion complex is not identical. When examining the surface projection of the outermost layer (Figure 4(a) and (f)), the capsomers now appear less well-defined than those in the CaMV reconstruction. Moreover, as shown in Figure 4(b) and (g), new densities are observed inside the pores surrounding the capsomers. These new densities are more pronounced when examining the sectioned views of the two reconstructions (Figure 4(c) and (h)). The radial projection at the outermost layer level clearly shows extra densities between capsomers (Figure 4(d) and (i)). Similarly, at the external level of the intermediate layer, which corresponds to a radius of 200 Å, extra densities appear in the center of the trimer-like motifs (arrows in Figure 4(e) and (j)).

Table 1. Structural data

Layer	CaMV average radius (Å)	P3:CaMV average radius (Å)	Swelling factor
Innermost	155	155	1.00
Intermediate	186	190	1.02 (2%)
Outermost	227	235	1.03 (3%)

Difference map between native and P3-decorated virions

In the present case, computing a difference map is not a straightforward process, since a swelling of the CaMV virion is observed when decorated with P3. Indeed, we showed that swelling factors of 3% and 2% were determined for the outermost and intermediate layers, respectively. The comparison of 3D reconstructions of native and P3-decorated CaMV particle showed clearly that the binding of P3 is reflected by the addition of extra densities in the outermost layer between the capsomers and in the intermediate layer, suggesting that P3 penetrates inside the viral capsid. Thus, the observed CaMV swelling when decorated with P3 is a real swelling of the CaMV viral particle and not the result of adding the density of P3 proteins on the outermost surface. We postulated that the CaMV swelling when decorated with P3 is induced by a relaxation of interactions between P4 proteins, allowing binding of P3 proteins, and not a reorganization of P4 proteins' structure. This assumption is defended by the fact that capsomers have the same shape in both maps. So, we decided to apply a scale factor of 3% to the CaMV density map prior to calculating the difference map with the P3–CaMV density map. As mentioned previously, the CaMV intermediate layer swells by 2% upon binding of P3, consequently a 3% artificial swelling of the CaMV reconstruction will introduce artefacts in the region of the intermediate layer. Accordingly, we decided to exclude the densities in the difference map at the surface level of the intermediate layer and below. This difference map was then merged with the reconstruction of the swollen CaMV particle (Figure 5). The virion shell surface is represented in yellow and the difference map in blue. No extra density is observed at the top of capsomers. The main difference when P3 interacts with virus particles is the appearance of new densities having an elongated shape of about 56 Å long and 22 Å wide, and joining capsomers. These rod-like motifs, which we call digitations, do not protrude out from the viral capsid but form a lateral network

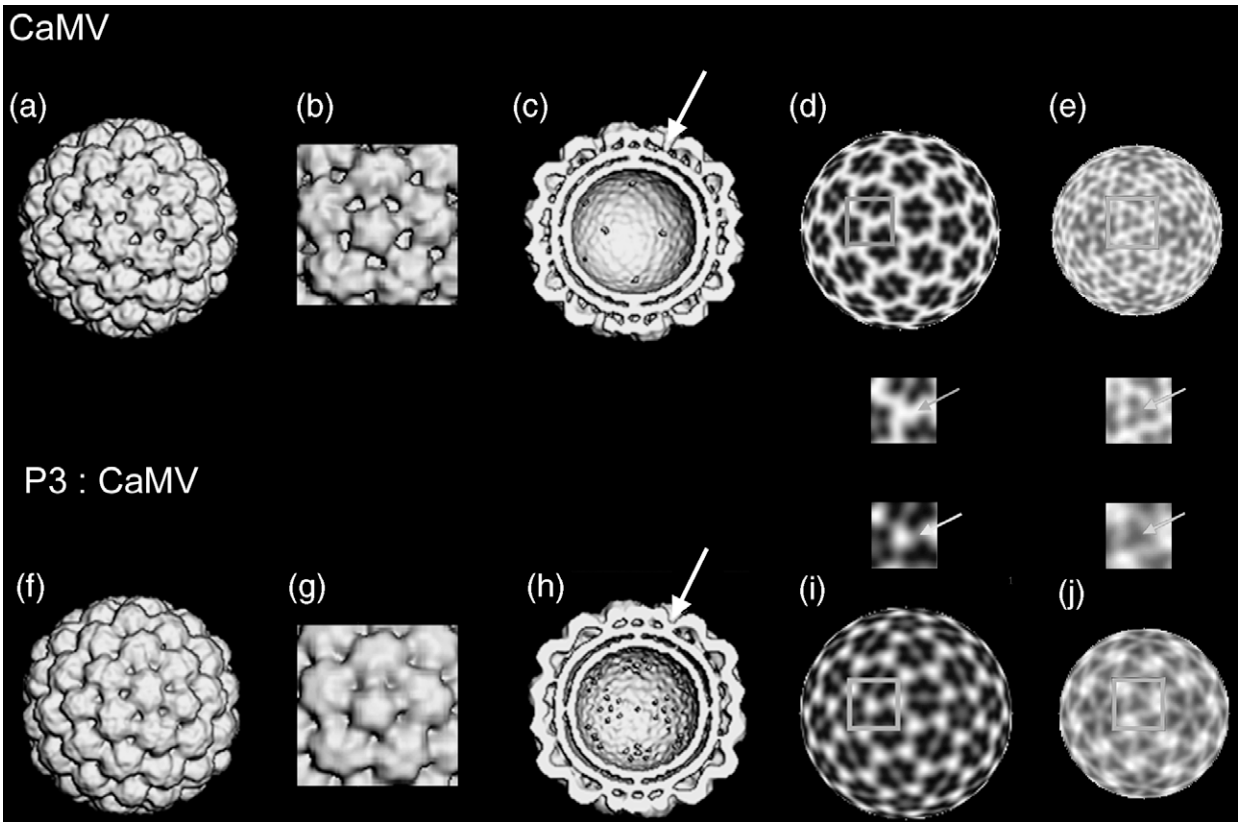

Figure 4. Three-dimensional reconstructions of native virions and P3:virion complex. The upper and lower rows correspond to different views of the virion and P3:virion complex reconstructions, respectively. (a) and (f) Surface representation viewed along a 2-fold axis. (b) and (g) Surface representation of one pentameric capsomer surrounded by five hexameric capsomers. The capsomers show distinct lumps according to the number of subunits and the pores around them seem to be filled upon binding of P3 onto the capsid. (c) and (h) Cutaway surface representation of the back half virion viewed along the same 2-fold axis as (a) and (f). Arrows indicate the position of additional density due to binding of P3. (d), (e), (i) and (j) Constant radius sections of the capsid corresponding to a radius of (d) and (i) 243 Å and (e) and (j) 200 Å. The grey-contoured regions are zoomed in the insets and arrows point to the position where additional density is observed in the P3:virion complex.

at its surface. As shown in the insets in Figure 5(b) and (d), two types of organisation exist between digitations and capsomers on the outermost layer of the capsid: digitations that establish connections between adjacent subunits of two hexamers and digitations connecting one hexamer and one pentamer. Each digitation is connected at both sides with compact domains, filling the pores surrounding the capsomers, and which we term anchoring domain. These anchoring domains are all linked on the outside to three digitations, and they deepen and traverse the outermost layer and fuse with the intermediate layer.

The most obvious motif visible seems to be formed by three semi-digitations surrounding an anchoring domain and forming a triskelion motif (Figure 5(c)). The asymmetric unit in the difference map that satisfies symmetry rules is composed of one digitation extended at both sides by one-third of an anchoring domain (Figure 5(e)). A pseudo-2-fold axial symmetry is located in the middle and perpendicular to the major axis of the digitation.

The N-terminal extremity of P3 is surface-exposed in the P3–virion complex

To determine the orientation of P3 in the digitations of the difference map, we purified virus particles and produced recombinant N and C-terminally His-tagged P3 (designated HP3 and P3H, respectively) as described in Materials and Methods. Virions were mixed together with HP3 or P3H extracts, and the mixture was applied to Ni-NTA resin to achieve co-purification. Figure 6(a) shows that unattached or excess HP3/P3H and virions, present in the original mixture, were detected in the unbound fractions but not in the last rinses. When bound proteins were eluted from the resin, co-purification of virus particles was efficient with HP3 but not with P3H. This observation could be explained in two different ways: (i) there is no interaction between virions and P3H and no complexes are formed; or (ii) the complexes do form but the His-tag at the C terminus of P3H is not accessible for binding. To distinguish between these two possibilities, we

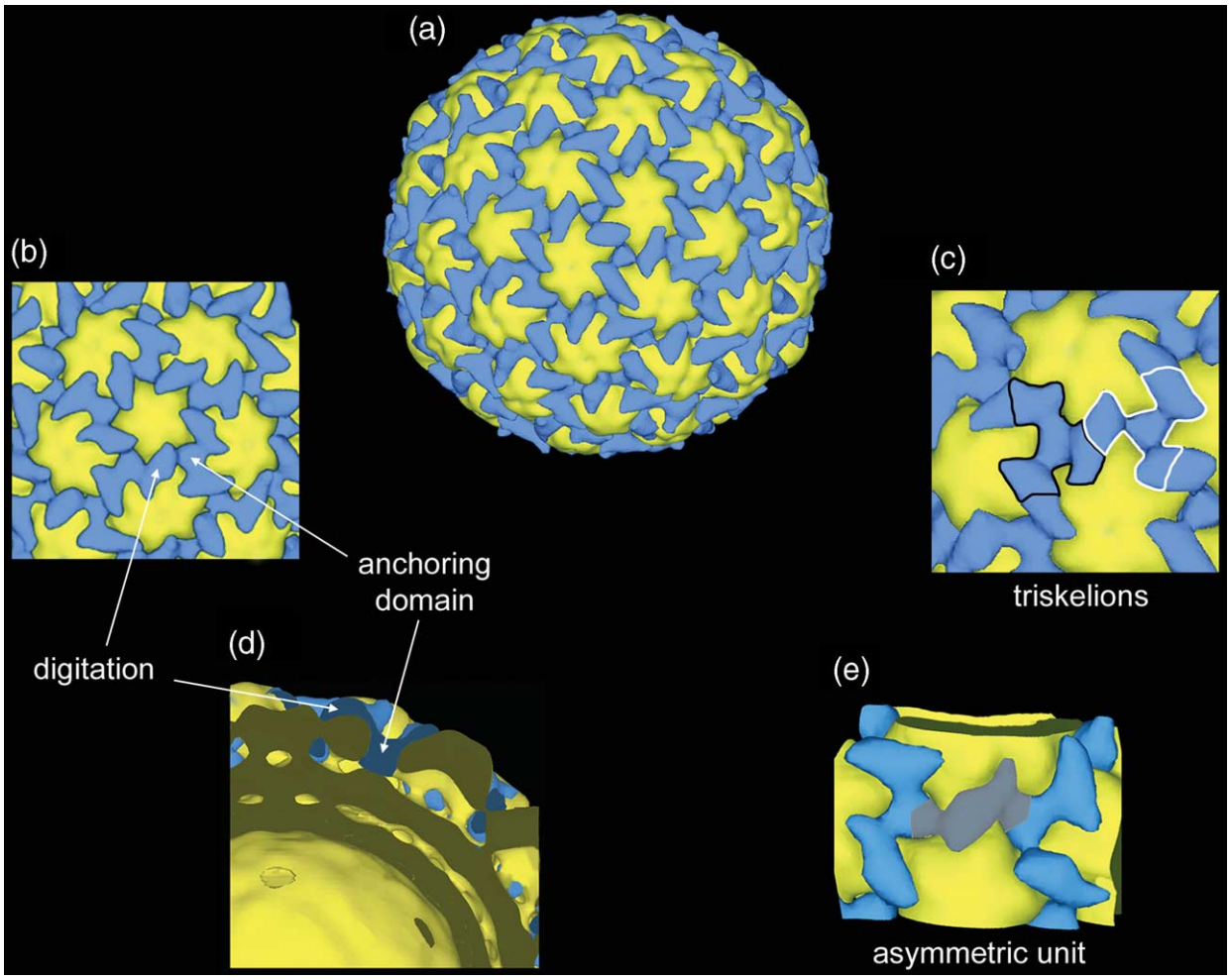

Figure 5. Visualization of the difference map. The surface representation of the CaMV virion is displayed in yellow and the difference map in blue. (a) Surface representation viewed along the 2-fold axis. (b) Surface representation of one pentameric capsomer surrounded by five hexameric CaMV capsomers. One digitation of the difference map links two hexameric capsomers or one hexameric and one pentameric capsomer. (c) Surface view of three adjacent hexamers of the CaMV capsid. Two triskelion motifs of the difference map are contoured in black and white. (d) Cutaway view of the top-right quarter of the P3:virion complex viewed along the same 2-fold axis as (a) and showing the anchoring domain penetrating the outer shell. (e) Surface representation of two adjacent triskelions of the difference map. One asymmetric unit is shadowed in grey.

assessed the virion-binding capacity of P3, HP3 and P3H using a protein–protein overlay assay as described.[14,15] As shown in Figure 6(b), both HP3 and P3H interacted with virus particles in a way comparable with wild-type P3, whereas the negative control P3Δ61-80, where P3 is deleted of part of its virus-binding domain,[8] displayed no detectable interaction.

From these results, we conclude that both HP3 and P3H form a complex with the virus particle and that, in these complexes, the N-terminal extremity of P3 is exposed and accessible to the solvent, whereas the C-terminal extremity is not and may be buried in the virus particle.

Discussion

Despite accumulating evidence that the P3-virion complex plays a pivotal role in the CaMV life-cycle, structural information has been totally lacking. Here, we report the structure of this complex at 26 Å resolution. Most importantly, as discussed below, the combination of our results with previously published data on biochemical and biological properties of P3 allows us to identify P3 molecules in the complex, to calculate the P3/P4 stoichiometry, and to hypothesise how P3 might specifically direct CaMV through diverse steps of the infection cycle.

Three-dimensional reconstructions obtained from frozen-hydrated virions showed that both native and P3-decorated virions are organised in three concentric layers surrounding a large and empty core. These CaMV structural features are similar to those recorded at 30 Å resolution.[6] Our maps indicate clearly that P3 binds to CaMV particles between capsomers, as shown by the

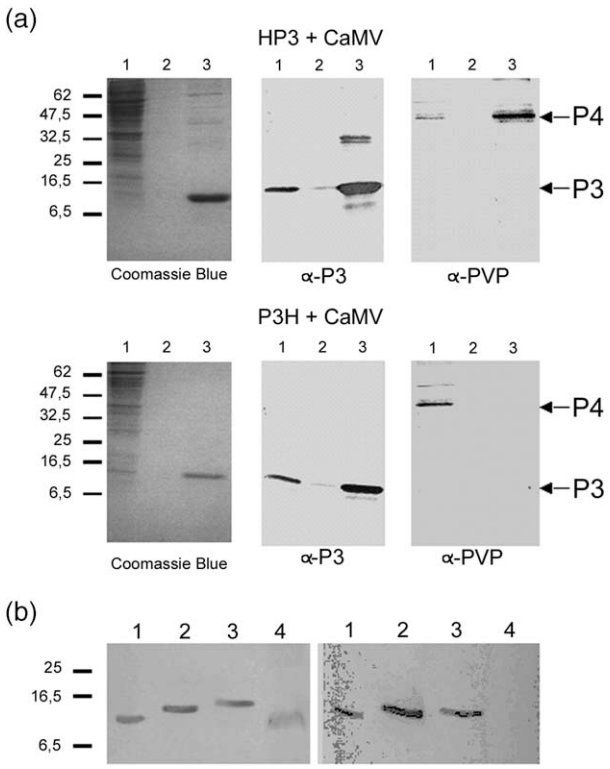

Figure 6. Binding and co-purification of virions with P3, HP3 and P3H. (a) Co-purification of virions and HP3 or P3H. Mixtures of virions and either HP3 or P3H were submitted to affinity purification on Ni-NTA resin as described in Materials and Methods. Various fractions were analysed by SDS/15% PAGE and stained with Coomassie brilliant blue or transferred onto nitrocellulose membranes prior to immunodetection of the proteins with an anti-P3 or anti-P4 serum. The gel was loaded as follows: lanes 1, unbound fractions; lanes 2, last rinses; lanes 3, eluted fractions. The molecular mass marker scales are indicated at the left. (b) Binding between virions and P3 or P3-derivatives. Samples (10 µl) of crude extracts from *Sf9* cells expressing P3 (positive control, lanes 1), HP3 (lanes 2) and P3H (lanes 3), and 5 µg of bacteria-expressed P3Δ61–80 (lanes 4, negative control, kindly provided by E. Jacquot & M. Keller)[8] were separated by SDS/15% PAGE. After transfer onto nitrocellulose membranes, P3 and derivatives were either revealed with anti-P3 serum (left panel), or (right panel) incubated with virions. After rigorous rinsing, bound virions were detected with an anti-P4 serum.

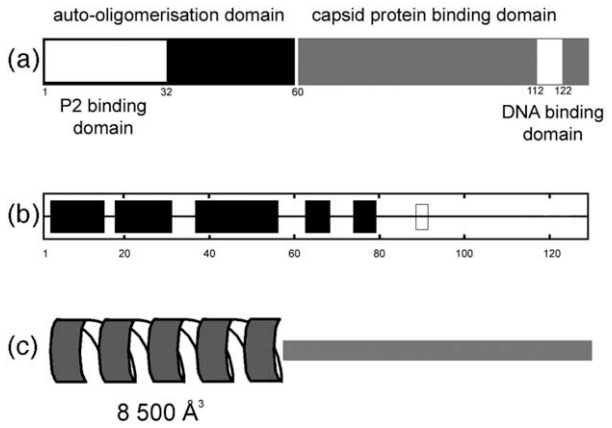

Figure 7. Alignment of biological functions, secondary structure prediction and structural domains of P3. (a) Previously reported mapping of functional regions in the P3 sequence. (b) P3 secondary structure as predicted by the Hnn program.[33] The predicted α-helical regions are displayed as black boxes and the predicted β-sheets as white boxes. (c) Estimated volume of the 60 N-terminal amino acid residues responsible for both P3–P3 and P3–P2 associations and forming coiled-coil interactions.

additional densities adjacent to the capsomers in the P3–virion complex as well as additional densities that appear inside the pores surrounding the capsomers. We conclude that P3 traverses the outermost layer and penetrates the intermediate layer, although we could not define the innermost limit of its extent. Thus, P3 binding on CaMV particle induces the appearance of a lateral network of digitations surrounding capsomers and extending to the inner layers by anchoring domains located inside capsid pores.

These data have to be related to previously published data that allowed mapping of various functions and/or properties of P3 in its primary sequence (Figure 7(a)). P3 appears to be divided into two functional[8] and structural domains:[20] an N-terminal domain of about 60 amino acid residues involved in self-organisation[20,21] and in interaction with P2,[14,15] and a C-terminal domain including residues 61–129 involved in the binding of P3 on the CaMV capsid.[14,21] A region located between residues 112 and 122 of this C-terminal domain has been demonstrated to possess non-specific DNA-binding activity.[8] Interestingly, the double-stranded DNA appears to be in close contact with the virus coat. A model has been proposed on the basis of neutron solution scattering experiments,[6,7] in which the DNA is located in the intermediate and inner layers of the virus shell.

The region of P3 responsible for both self-organisation and P2-binding consists of the first 60 N-terminal amino acid residues. Secondary structure prediction (Figure 7(b)) assigns this region with a high probability to be composed of α-helices. Besides, Leh *et al*. showed that both P3-P3 and P3-P2 associations are formed by N-terminal coiled-coil interactions.[15] Thus, compact rod-like domains are expected. These structural features are present in our difference map with the rod-like domains that we called digitations. This suggests that external and exposed digitations are composed of one or more P3 N-terminal regions, whereas the anchoring domains, putatively interacting with the encapsidated DNA, are composed of sequences located at the C-terminal portion of P3. This is fully consistent with our results obtained with co-purification of virions and His-tagged P3 mutants, which indicate that the N terminus of P3 is surface-exposed while the C terminus is buried in the virion. It is worth

Table 2. Influence of threshold values for displaying the difference map scooped out at radius 239 Å

	Threshold average	Threshold average +1σ	Threshold average +2σ	Threshold average +3σ
Volume/digitation (Å^3)	28,885	23,131	18,838	15,081
No. P3 N-terminal 60 residues/digitation	3.4	2.7	2.2	1.8
Stoichiometry P3/P4	1.7	1.35	1.1	0.9

The average corresponds to the average of the map density. σ, standard deviation.

mentioning that the repeated unit (Figure 5(e)) is composed of a pseudo-2-fold axial symmetry located in the middle of a digitation, which implies that the digitations are composed of an even number of P3 N-terminal regions.

The assessment of the volume of one digitation is closely related to the threshold value applied to the difference map. Moreover, the choice of a threshold value is quite ambiguous without internal reference. Commonly, the threshold value used to display a density map is the average density plus twice the standard deviation. To consider only the contribution of digitations, we scooped out the difference map at the radius of 239 Å, then various threshold values were considered and the volume corresponding to one digitation determined (Table 2). From the Table describing the volumes occupied by amino acids in solution[22] or from a coiled-coil organisation model, the theoretical volume estimated for the P3 N-terminal 60 amino acid residues is about 8500 Å^3 (Figure 7(c)). This value was used to estimate the number of P3 N-terminal 60 amino acid residues per digitation (Table 2). As digitations are composed of an even number of P3 N-terminal regions, the most likely possibility is that one digitation is formed by the association of N-terminal extremities from two P3 molecules. With respect to the number of digitations, a stoichiometry of one P3 molecule for one P4 molecule is expected. Moreover, considering the volume of the difference map with a density threshold value of the average plus two standard deviations (which gave two P3 N-terminal 60 amino acid residues per digitation), a volume of 7.2 E6 Å^3 is obtained. Since the theoretical volume occupied by one P3 molecule is 18,180 Å^3, the difference map should contain 396 P3 molecules. This number is close to 420, which corresponds to a stoichiometry of 1 : 1 for the P3/P4 ratio. The error is of 5.7% but it should be mentioned that some additional densities resulting from P3 binding on the CaMV intermediate layer were not taken into account in the difference map. In conclusion, this study suggests strongly a stoichiometry of one P3 molecule for one P4 molecule. This is consistent with the observation that the excess of soluble P3 appeared with P3/P4 ratios comprised between 1 : 1 and 2 : 1. Consequently, as the digitations are formed by two P3 60 N-terminal amino acid residues, the anchoring domain results from the association of three P3 monomers. The C-terminal part of P3 being involved in interactions with both the CaMV capsid and with the nucleic acid, it seems reasonable to assume that it can easily penetrate the intermediate layer of the shell to gain proximity with the DNA present at these levels. The DNA-binding extreme C terminus of P3 could control its attachment and orientation on the capsid.

The consistency discussed above between our biochemical and structural data, the secondary structure prediction, and previously published information of the biological properties of P3 allow us to propose a structural model of the CaMV P3–virion complex (Figure 8). P3 is a dimer when bound to the CaMV capsid. Antiparallel, coiled-coil dimerization of N-terminal sequences on the surface of the virus explains best the shape and volume of the digitations. Groups of three C-terminal extremities interact with the coat protein, penetrate the CaMV shell through pores and settle in the intermediate layer where they possibly interact with the viral DNA.

It has been shown that P3 forms a tetramer in solution.[20,23,24] Our results imply an alternative conformation of P3 when attached to virions, changing from an N-terminal tetramer to an N-terminal dimer. Our proposed model is in agreement with the mechanisms of CaMV acquisition by aphids described previously.[13] Those authors found that, out of the cellular context, P2 interacted only with virion-bound P3 and not with free P3, and that the kinetics of P3 binding to the virus were suggestive of a conformational change of P3. We propose that the tetrameric organisation of

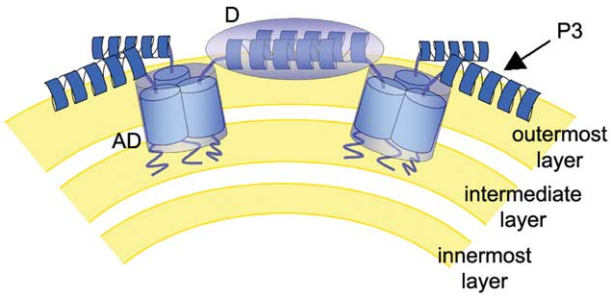

Figure 8. Interaction model of P3 with CaMV capsid. P3 is present as a dimer when binding the CaMV capsid by interaction of N-terminal sequences, forming digitation (D domain). The anchoring domain (AD domain) consists of the association of three P3 monomers. The C-terminal part of P3 penetrates the intermediate layer of the shell and then interacts with both the CaMV capsid and the nucleic acid.

soluble P3 masks the P2 interaction sites that are contained in the P3 N-terminal coiled-coil. Upon binding of P3 to the virus particle and the concomitant change to a dimeric form, the P2-binding sites would become exposed and accessible to P2. Thus, the oligomerization state of P3 might regulate its activity, at least concerning P2. A 3D reconstruction of the entire P2:P3:CaMV complex by microscopy and image analysis should help to better resolve the nature of these interactions.

Such a conformational change suggests how the multiple functionality of P3 would depend on its oligomerization state, as postulated previously.[21,23] What we further propose here is that this could be true also for virion-bound P3, which could act as the "arms" of the virus particle, by keeping its C terminus anchored into the capsid shell and, depending on the oligomerization status of the exposed N terminus, could have different targets engaging the complex in various pathways throughout the infection cycle. One such pathway has already been demonstrated for aphid transmission, where P3 forms a network of P2 interaction sites at the surface of the virion shell. Two assumptions can be postulated for P2–P3 interaction: either P2 binds directly to the P3 N-terminal dimer or P2 interacts with a monomer of P3, which would require dissociation of the digitations. The similar phenomenon will likely be observed for cell-to-cell or long-distance movement. The recent discoveries that P3 is required for virus movement in the host plant,[17] and that P1 (the CaMV movement protein) interacts with the N terminus of P3 *via* formation of coiled-coil structures (L. Stavolone and T. Hohn, personal communication) fully support our hypothesis.

Materials and Methods

Expression and/or purification of CaMV, P3, HP3, P3H

CaMV virions (Cabb-S isolate) were purified from infected turnip leaves essentially as described,[15] with an additional centrifugation step through a 40–80% (w/v) sucrose gradient for 18 hours at 55,000 *g*. The virus-containing fraction was then supplemented with 10% (v/v, final concentration) butanol, incubated for ten minutes and centrifuged at 200,000 *g* for three hours. The pelleted virions were finally resuspended in 20 mM Tris–HCl (pH 6.9) supplemented with β-octylthioglucoside (βOG) at one critical micelle concentration (CMC), and stored at 4 °C. Virus concentration was estimated by spectrometry using the formula described by Hull *et al*.[25]

The baculovirus recombinants expressing His-tagged P3 in N-terminal (HP3) and in C-terminal (P3H) were obtained exactly as described for those expressing HP2 and P2H,[26] except that the primers for PCR-amplification and cloning were adapted to match the ORF III 5′ and 3′ sequences, instead of those of ORF II. The full sequences of *p119His* plasmid[26] and primers are available on request. The conditions for expressing P3, HP3 and P3H in the baculovirus/insect cell system were as described.[13] The crude extracts used in this study were prepared from *Sf9* cells infected with P3, HP3 or P3H in a 75 cm^2 culture flask (Falcon). The cells were pelleted and resuspended in 1 ml of P3 buffer (20 mM Tris–HCl (pH 8.0), 200 mM NaCl) supplemented with Complete Antiprotease Cocktail (Roche Diagnostics).

For reconstitution of P3:virion complexes for cryo-electron microscopy, large amounts of P3 were produced and purified from the bacterial clone pETCa3.[8] IPTG-induced cells were resuspended in P3-antiprotease buffer and disrupted by ultrasonication. The soluble fraction was treated at 65 °C for ten minutes, and centrifuged at 20,000 *g* to remove denatured proteins. Heat-stable P3, in the supernatant, was then purified by differential precipitation using increasing concentrations of ammonium sulfate, and resuspended in P3 buffer. Remaining traces of ammonium sulfate were removed by dialysis, and the concentration of P3 was measured by spectrometry.

Binding and co-purification of virions and P3 or derivatives

The virion binding assays were performed as described,[14] and the same antibodies against P3 and P4 were used. For co-purification of virions with HP3 or P3H, Ni-NTA resin was incubated with a mixture of HP3 or P3H crude extracts and 100 μg of purified virions for one hour at 4 °C, in 10 ml of CaMV buffer (20 mM Tris–HCl (pH 7.2) with βOG at 1 CMC). The resin was sedimented at 10,000 *g* for five minutes and rinsed three times with 1.5 ml of P3 buffer, bound proteins and complexes were then eluted using 0.5 ml of P3 buffer supplemented with 300 mM imidazole.

Preparation of samples for cryo-electron microscopy

For preparation of P3:virion complexes, CaMV virions and P3 were incubated at a molecular ratio of 1.5 : 1 (P3/P4) under gentle stirring at 4 °C for 24–48 hours in CaMV buffer. Final concentration of the complex was estimated to be about 1 mg/ml. Due to agregation of P3–CaMV particle complexes during centrifugation, excess free P3 was not removed. For both native and P3-decorated virions, βOG was removed from the solution by using SM2 biobeads (Biorad). Samples (3 μl) of CaMV virions or complexes were applied to holey carbon grids, blotted with filter-paper for 2–3 seconds and vitrified in liquid ethane. Specimens were transferred into a 200 kV FEG electron microscope (JEOL 2010F) with a Gatan 626 cryo-holder. Focal pairs of images were recorded under low-dose conditions at a magnification of 39,600× with 0.6 μm and 1.2 μm underfocus. The magnification was calibrated using the 23 Å layer-line of tobacco mosaic virus.

Image processing and three-dimensional reconstructions

Electron micrographs were digitised with a Hi-scan scanner (Eurocore) at 15 μm/pixel, corresponding to a nominal pixel size of 3.79 Å. Data were processed as described.[27] Briefly, the semi-automatic X3D program (J. F. Conway) was used for picking particles. The defocus value was estimated for each micrograph. Images were corrected for contrast transfer effects, and focal pairs of images were combined using the SUMPS and CTFMIX programs.[27]

Particle origins and orientations were determined and refined using the model-based orientation determination method.[19] The CaMV reconstruction was determined

using as starting model the 3D reconstruction of the $T=7$ bacteriophage HK97 prohead I computed at 40 Å resolution.[28] After two refinement cycles, the computed model had the overall structural features of CaMV obtained by Cheng *et al*.[6] This new model was then used as reference for the other refinement cycles. In the case of P3–CaMV particle complexes, the starting model was our CaMV reconstruction computed at 40 Å resolution, rescaled to match with P3–CaMV viral particles, and scooped out in order to include only the outermost layer. Using the $T=7$ bacteriophage HK97 prohead I as the starting model gave the same results with one more refinement cycle. The final density maps included particles from different focal pairs or single images: 653 particles from four focal pairs for the reconstruction of the CaMV capsid and 1484 particles from six focal pairs and two single images for the P3–CaMV complex. In both reconstructions, the distribution of particle orientations gave a good coverage of the icosahedral asymmetric unit (data not shown). Density maps were calculated by Fourier-Bessel formalism as described,[29] and implemented in the EM3DR program of T. Baker. Resolution was estimated using the Fourier shell correlation (FSC) criterion with a cutting level of 0.5 ($FSC_{0.5}$).[30,31] With respect to the final resolution and the level of interpretation, handedness of capsids was not determined but was arbitrarily assigned as $T=7$ *laevo*. We determined 3D reconstructions of CaMV and P3–CaMV complex at 18 Å and 26 Å, respectively. To allow for structural comparisons between native and P3–CaMV complexes, the 3D reconstructions were calculated to 26 Å resolution. The raw radial density profiles were computed by spherically averaging both 3D reconstructions calculated at 26 Å resolution. The density maps were normalized by using the density peak located at 155 Å as reference. Comparison of the normalised radial density profiles indicated that the swelling factor of the CaMV capsid induced by the binding of P3 is different for the concentric capsid layers (see Table 1). As explained in Results, a scale factor of 3% was applied to the CaMV density map. Then, a difference map between P3–CaMV and CaMV density maps was calculated using the programs RobEM (R. Ashmore & T. Baker, unpublished) and Bsoft.[32] However, the CaMV intermediate layer swells by 2% upon binding of P3. So, the difference map induces artefacts in the region of the intermediate layer. Consequently, the difference map was truncated at the surface of the intermediate layer of virions and below. For displaying the CaMV map, the cutoff level was chosen so that the volume enclosed by the isosurface corresponded to the predicted mass of the particle (420×37–42 kDa). In the other cases, the density threshold value used for displaying maps corresponds to the average density plus twice the standard deviation.

Acknowledgements

Images were recorded at the CNRS—Pasteur Institut Federative Microscope. We thank G. Pehau-Arnaudet for assistance with electron microscopy. The work was supported, in part, by a grant from the M.E.S.R. to C.P. The P3Δ61–80 and pETCa3 were kindly provided by E. Jacquot and M. Keller.

References

1. Rothnie, H. M., Chapdelaine, Y. & Hohn, T. (1994). Pararetroviruses and retroviruses: a comparative review of viral structure and gene expression strategies. *Advan. Virus Res.* **44**, 1–67.
2. Jacquot, E., Geldreich, A., Keller, M. & Yot, P. (1997). Les pararétrovirus de plante. *Virologie*, **1**, 111–121.
3. Hohn, T. & Fütterer, J. (1997). The proteins and functions of plant pararetroviruses: knowns and unknowns. *Crit. Rev. Plant Sci.* **16**, 133–167.
4. Kiss-Laszlo, Z., Blanc, S. & Hohn, T. (1995). Splicing of cauliflower mosaic virus 35 S RNA is essential for viral infectivity. *EMBO J.* **14**, 3552–3562.
5. Chauvin, C., Jacrot, B., Lebeurier, G. & Hirth, L. (1979). The structure of cauliflower mosaic virus: a neutron diffraction study. *Virology*, **96**, 640–641.
6. Cheng, R. H., Olson, N. H. & Baker, T. S. (1992). Cauliflower mosaic virus: a 420 subunit ($T=7$), multilayer structure. *Virology*, **186**, 655–668.
7. Kruse, J., Timmins, P. & Witz, J. (1987). The spherically averaged structure of a DNA isometric plant virus: cauliflower mosaic virus. *Virology*, **159**, 166–168.
8. Jacquot, E., Geldreich, A., Keller, M. & Yot, P. (1998). Mapping regions of the cauliflower mosaic virus ORF III product required for infectivity. *Virology*, **242**, 395–402.
9. Mesnard, J. M., Kirchherr, D., Wurch, T. & Lebeurier, G. (1990). The cauliflower mosaic virus gene III product is a non-sequence-specific DNA binding protein. *Virology*, **174**, 622–624.
10. Giband, M., Mensard, J.-M. & Lebeurier, G. (1986). The gene III product (P15) of cauliflower mosaic virus is a DNA-binding protein while an immunologically related P11 polypeptide is associated with virions. *EMBO J.* **5**, 2433–2438.
11. Mougeot, J. L., Guidasci, T., Wurch, T., Lebeurier, G. & Mesnard, J. M. (1993). Identification of C-terminal amino acid residues of cauliflower mosaic virus open reading frame III protein responsible for its DNA binding activity. *Proc. Natl Acad. Sci. USA*, **90**, 1470–1473.
12. Dautel, S., Guidasci, T., Pique, M., Mougeot, J. L., Lebeurier, G., Yot, P. & Mesnard, J. M. (1994). The full-length product of cauliflower mosaic virus open reading frame III is associated with the viral particle. *Virology*, **202**, 1043–1045.
13. Drucker, M., Froissart, R., Hebrard, E., Uzest, M., Ravallec, M., Esperandieu, P. *et al*. (2002). Intracellular distribution of viral gene products regulates a complex mechanism of cauliflower mosaic virus acquisition by its aphid vector. *Proc. Natl Acad. Sci. USA*, **99**, 2422–2427.
14. Leh, V., Jacquot, E., Geldreich, A., Haas, M., Blanc, S., Keller, M. & Yot, P. (2001). Interaction between the open reading frame III product and the coat protein is required for transmission of cauliflower mosaic virus by aphids. *J. Virol.* **75**, 100–106.
15. Leh, V., Jacquot, E., Geldreich, A., Hermann, T., Leclerc, D., Cerutti, M. *et al*. (1999). Aphid transmission of cauliflower mosaic virus requires the viral PIII protein. *EMBO J.* **18**, 7077–7085.
16. Palacios, I., Drucker, M., Blanc, S., Leite, S., Moreno, A. & Fereres, A. (2002). Cauliflower mosaic virus is preferentially acquired from the phloem by its aphid vectors. *J. Gen. Virol.* **83**, 3163–3171.
17. Kobayashi, K., Tsuge, S., Stavolone, L. & Hohn, T.

(2002). The cauliflower mosaic virus virion-associated protein is dispensable for viral replication in single cells. *J. Virol.* **76**, 9457–9464.
18. Blanc, S., Hebrard, E., Drucker, M. & Froissart, R. (2001). Molecular basis of vector transmission: caulimoviruses. In *Virus-Insect-Plant Interactions* (Harris, K., Smith, O. P. & Duffus, J. E., eds), pp. 143–146, Academic Press, San Diego.
19. Baker, T. S. & Cheng, R. H. (1996). A model-based approach for determining orientations of biological macromolecules imaged by cryoelectron microscopy. *J. Struct. Biol.* **116**, 120–130.
20. Leclerc, D., Burri, L., Kajava, A. V., Mougeot, J. L., Hess, D., Lustig, A. *et al*. (1998). The open reading frame III product of cauliflower mosaic virus forms a tetramer through a N-terminal coiled-coil. *J. Biol. Chem.* **273**, 29015–29021.
21. Leclerc, D., Stavolone, L., Meier, E., Guerra-Peraza, O., Herzog, E. & Hohn, T. (2001). The product of ORF III in cauliflower mosaic virus interacts with the viral coat protein through its C-terminal proline rich domain. *Virus Genes*, **22**, 159–165.
22. Chothia, C. (1984). Principles that determine the structure of proteins. *Annu. Rev. Biochem.* **53**, 537–572.
23. Stavolone, L., Herzog, E., Leclerc, D. & Hohn, T. (2001). Tetramerization is a conserved feature of the virion-associated protein in plant pararetroviruses. *J. Virol.* **75**, 7739–7743.
24. Tsuge, S., Kobayashi, K., Nakayashiki, H., Mise, K. & Furusawa, I. (1999). Cauliflower mosaic virus ORF III product forms a tetramer in planta: its implication in viral DNA folding during encapsidation. *Microbiol. Immunol.* **43**, 773–780.
25. Hull, R., Shepherd, R. J. & Harvey, J. D. (1976). Cauliflower mosaic virus: an improved purification procedure and some properties of the virus particle. *J. Gen. Virol.* **31**, 93–100.
26. Hebrard, E., Drucker, M., Leclerc, D., Hohn, T., Uzest, M., Froissart, R. *et al*. (2001). Biochemical characterization of the helper component of cauliflower mosaic virus. *J. Virol.* **75**, 8538–8546.
27. Conway, J. F. & Steven, A. C. (1999). Methods for reconstructing density maps of "single" particles from cryoelectron micrographs to subnanometer resolution. *J. Struct. Biol.* **128**, 106–118.
28. Conway, J. F., Duda, R. L., Cheng, N., Hendrix, R. W. & Steven, A. C. (1995). Proteolytic and conformational control of virus capsid maturation: the bacteriophage HK97 system. *J. Mol. Biol.* **253**, 86–99.
29. Crowther, R. A. (1971). Procedures for three-dimensional reconstructions of spherical viruses by Fourier synthesis from electron micrographs. *Phil. Trans. Roy. Soc. London*, **261**, 221–230.
30. Van Heel, M. (1987). Angular reconstitution: a posteriori assignment of projection directions for 3D reconstruction. *Ultramicroscopy,* **21**, 111–123.
31. Saxton, W. O. & Baumeister, W. (1982). The correlation averaging of a regularly arranged bacterial cell envelope protein. *J. Microsc.* **127**, 127–138.
32. Heymann, J. B. (2001). Bsoft: image and molecular processing in electron microscopy. *J. Struct. Biol.* **133**, 156–169.
33. Combet, C., Blanchet, C., Geourjon, C. & Deleage, G. (2000). NPS@: network protein sequence analysis. *Trends Biochem. Sci.* **25**, 147–150.

Edited by W. Baumeister

(Received 23 July 2004; received in revised form 15 November 2004; accepted 17 November 2004)